Inorganic Chemistry

Article

pubs.acs.org/IC

Magnetic Properties of $CeMn_{2-x}Co_xGe_4O_{12}$ ($0 \leq x \leq 2$) as a Function of Temperature and Magnetic Field

Diming Xu,[†] Maxim Avdeev,[‡,§] Peter D. Battle,*[,†] and Xiao-Qiang Liu[∥]

[†]Inorganic Chemistry Laboratory, Oxford University, South Parks Road, Oxford OX1 3QR, U. K.

[‡]Australian Nuclear Science and Technology Organisation, Lucas Heights, NSW 2234, Australia

[§]School of Chemistry, The University of Sydney, Sydney, NSW 2006, Australia

[∥]School of Materials Science and Engineering, Zhejiang University, 38 Zheda Road, Hangzhou 310027, China

ABSTRACT: Polycrystalline samples, prepared by a solid-state route, of compositions in the solid solution $CeMn_{2-x}Co_xGe_4O_{12}$ (x = 0.0, 0.5, 1.0, 1.5, and 2.0) were characterized by X-ray diffraction, neutron diffraction, and magnetometry. They adopt space group $P4/nbm$ with $a \approx 9.78$ and $c \approx 4.85$ Å and become anti-ferromagnetic (x = 0.0, 1.5, 2.0) or weakly ferromagnetic (x = 0.5, 1.0) at $4.2 \leq T \leq 7.6$ K. The ordered moments lie along [001] when x = 0.0 and in the (001) plane otherwise. The unit cell doubles along [001] when x = 1.5 and 2.0 order anti-ferromagnetically, but the doubling is lost when a first-order metamagnetic transition to weak ferromagnetism occurs on the application of a 10 kOe magnetic field. The ordered moments at 1.6 K for x = 0.0 and 2.0 are 4.61(2) and 2.58(2) μ_B, respectively; the corresponding effective moments in the paramagnetic phase are 5.91 and 5.36 μ_B.

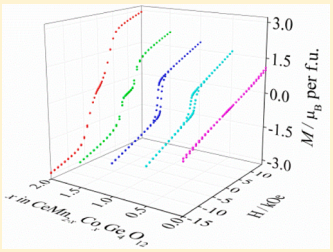

INTRODUCTION

Most studies of the occurrence of long-range magnetic ordering in inorganic compounds have focused on mixed-metal oxides. The dominant superexchange pathway in these materials is usually M−O−M′, where M and M′ are paramagnetic transition-metal cations. It has, however, also been shown that ordering can also occur in oxo-acid salts, for example, sulfates, molybdates, phosphates, and arsenates.[1−4] The superexchange pathway in these compounds is typically M−O−X−O−M′, where X is a nonmetal or a transition-metal cation with a d^0 electron configuration. The extended superexchange pathway, sometimes referred to as the supersuperexchange pathway, usually leads to relatively low transition temperatures, for example, 28 and 25 K in $Fe_2(SO_4)_3$ [3] and $FePO_4$,[1] respectively. It does not, however, preclude the observation of unusual magnetic behavior; $Fe_2(SO_4)_3$ was the first compound to show the L-type ferrimagnetism predicted by Néel in 1948.[5]

A number of germanates[6−16] are among the salts whose magnetic properties have been investigated in recent years. They include the triclinic phases $R_2CuGe_4O_{12}$ (where R represents a lanthanide or Y),[15,16] which order anti-ferromagnetically below 6 K. However, long-range magnetic order has not previously been observed in the somewhat different, tetragonal structure originally reported by Taviot-Guého et al.[17] and subsequently studied extensively during a search for materials that might have applications in photonics.[18−24] The majority of these compounds have the formula $R_2MGe_4O_{12}$, where R is a lanthanide or Y and M is Ca, Mn, or Zn. They crystallize in the space group $P4/nbm$ with the 2b site being occupied by the cation R and the 4f site by a disordered 1:1 distribution of R and M. The two distinct cation sites are coordinated by eight and six oxygen atoms, respectively, and have square-antiprismatic and octahedral geometries. They can be considered to lie in layers perpendicular to the [001] axis. These layers are separated from each other by layers containing $[Ge_4O_{12}]^{8-}$ rings, each ring being comprised of four vertex-sharing GeO_4 tetrahedra; see Figure 1. Our first attempts to introduce paramagnetic cations other than Mn^{2+} into the structure resulted in the synthesis of $Y_2CoGe_4O_{12}$.[25] This compound was shown to remain paramagnetic down to 2 K, but, interestingly, the effective magnetic moment of the Co^{2+} cations took the unusually large value of 6.05 μ_B. This was attributed to the presence of an enhanced orbital contribution to the magnetic moment as a consequence of the large pseudotetragonal strain at the Co^{2+} site. In an attempt to induce long-range magnetic ordering in this structure we have now begun to consider compositions in which all the six-coordinate 4f sites are occupied by magnetic cations, for example, $CeMn_2Ge_4O_{12}$. This $RM_2Ge_4O_{12}$ composition was described by Taviot-Guého et al.,[17] but no magnetic data were presented. We report below the preparation and characterization by magnetometry, X-ray diffraction, and neutron diffraction of $CeMn_2Ge_4O_{12}$ and other members of the solid solution $CeMn_{2-x}Co_xGe_4O_{12}$; the composition dependence of their magnetic behavior is more marked than that seen previously in $Sr_2MGe_2O_7$ (M = Mn, Co).[12]

EXPERIMENTAL SECTION

Polycrystalline samples of $CeMn_{2-x}Co_xGe_4O_{12}$ (x = 0.0, 0.5, 1.0, 1.5, and 2.0) were synthesized in solid-state reactions. Stoichiometric quantities of CeO_2 (99.99%), Co_3O_4 (99.9985%), $MnCO_3$ (99.985%), and GeO_2 (99.9999%) were mixed thoroughly in an agate mortar, along with a 10% excess of GeO_2 to counteract its loss at high

Received: December 2, 2016

DOI: 10.1021/acs.inorgchem.6b02905
Inorg. Chem. XXXX, XXX, XXX−XXX

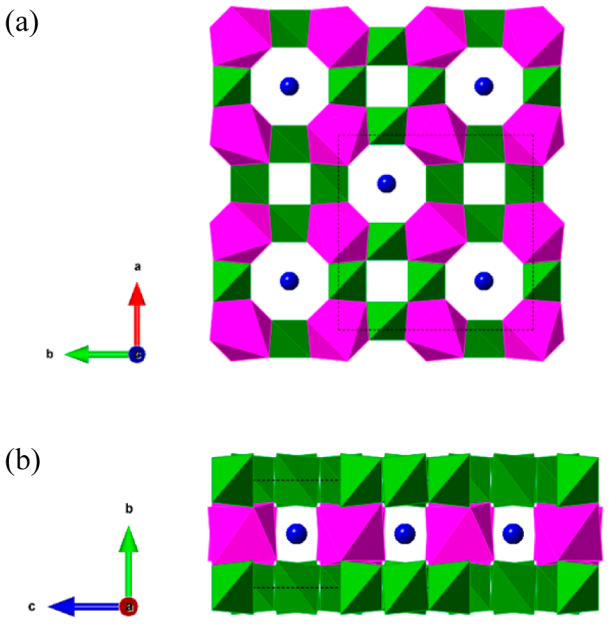

Figure 1. Polyhedral representation of the crystal structure of $CeMn_{2-x}Co_xGe_4O_{12}$ viewed along (a) [001] and (b) [100]: green tetrahedra and purple octahedra represent GeO_4 and $(Mn/Co)O_6$ groups, respectively; blue circles represent Ce^{4+} cations.

temperature. The mixtures were heated at 1075 °C for 7 d with intermediate cooling and regrinding every 2 d.

X-ray powder diffraction (XRPD) patterns were recorded at room temperature on a Panalytical X'pert diffractometer using Cu $K\alpha_1$ radiation. Data were collected in the angular range $10° \leq 2\theta \leq 130°$, with a step size of $\Delta 2\theta = 0.0084°$. Neutron powder diffraction (NPD) patterns were collected over the range of $8° \leq 2\theta \leq 160°$ using a step size of $\Delta 2\theta = 0.05°$ and a wavelength of either 1.622 or 2.4395 Å. The measurements were performed on the high-resolution powder diffractometer ECHIDNA at ANSTO. The data were analyzed by the Rietveld method[26] using the program GSAS[27] and the peak shape function developed by van Laar and Yelon.[28] For the majority of the measurements, the sample was loaded in powder form into a vanadium can that was mounted in a closed-cycle refrigerator. However, some patterns were collected with the sample mounted in a vertical-field cryomagnet. In these cases, to prevent movement in the magnetic field, the sample was pressed into a pellet that was subsequently broken into fragments, each just small enough to be loaded into a standard vanadium container. Regions of the diffraction profile that were contaminated by Bragg peaks from aluminum in the cryomagnet were excluded from the subsequent analysis. Data were collected in zero field, then in fields of up to 30 kOe. Finally the measurement in zero field was repeated to ensure that the application of a field had not caused preferred orientation of the powder granules.

Magnetic measurements were performed using a Quantum Design MPMS 5000 SQUID magnetometer. Direct-current (dc) susceptibility measurements were made on warming over the temperature range of $2 \leq T \leq 300$ K in an applied field of 100 Oe following both zero-field cooling (ZFC) and field-cooling (FC) of the sample. The field dependence of the magnetization was measured at 2 K over the field range of $-50 < H < 50$ kOe. Alternating-current (ac) susceptibilities were measured at frequencies up to 1 kHz over the temperature range of $2 \leq T \leq 10$ K in a 3.5 Oe ac field.

RESULTS

The sample of $CeCo_2Ge_4O_{12}$ was green in color, whereas the other four compositions were brown. An initial inspection of the XRPD patterns collected from the five samples specified above showed that all were dominated by the Bragg peaks expected for the target phase. These could be indexed in the

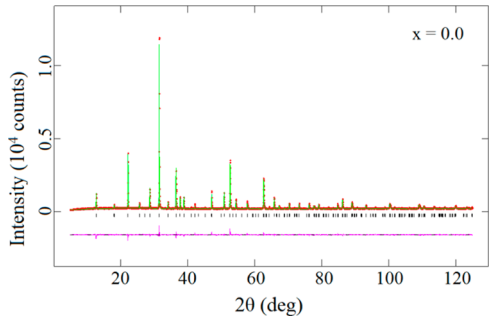

Figure 2. Observed (red dots) and calculated (green line) XRPD patterns of $CeMn_2Ge_4O_{12}$ at room temperature. A difference curve (purple line) is shown, and reflection positions are marked.

tetragonal space group $P4/nbm$ (No. 125) and were consistent with the structural model used previously to describe $Y_2CoGe_4O_{12}$.[25] The fitted pattern of $CeMn_2Ge_4O_{12}$ is shown in Figure 2. However, the patterns of $CeMn_{1.0}Co_{1.0}Ge_4O_{12}$ and $CeMn_{0.5}Co_{1.5}Ge_4O_{12}$ clearly contained weak, additional peaks attributable to a low level (~1%) of a CeO_2 impurity.

The temperature dependence of the dc molar susceptibility of each sample is shown in Figure 3. The parameters resulting from fitting the Curie–Weiss law to the data collected at $T > 150$ K are listed in Table 1, as is the temperature T_c of the transition that was observed in each case. The field dependence of the magnetization is also shown in Figure 3. Values of the coercive field H_c and remanent magnetization M_r are included in Table 1 as appropriate. In the light of these data, further susceptibility measurements were made in higher fields on the samples $x = 1.5$, 2.0; see Figure 4. For each sample, the temperature and frequency dependence of the ac molar susceptibility, measured in the absence of a dc field, is shown in Figure 5. To aid our interpretation of the dc susceptibility and $M(H)$ of $CeMn_2Ge_4O_{12}$ further ac measurements were performed in dc fields of 500 Oe and 20 kOe. These data are shown in Figure 6.

Neutron diffraction data were collected from each sample at room temperature and 1.6 K using a wavelength of $\lambda = 1.622$ Å. Initially, the data collected at room temperature were analyzed using a model containing the principal phase and, for $x = 1.0$ and 1.5, CeO_2. In the mixed manganese/cobalt compositions the two types of cation were found to occupy the 4f site in a disordered manner. The observed and calculated diffraction profiles of $CeMn_2Ge_4O_{12}$ are shown in Figure 7. All the patterns collected at 1.6 K contained additional Bragg peaks that were not observed at room temperature. The majority of these could be attributed to the onset of long-range magnetic order in the main phase. However, in the case of the compositions $x = 1.0$ and 1.5, some of the additional Bragg scattering was ascribed to magnetic scattering from a previously undetected impurity phase, orthorhombic $CoGeO_3$, which is anti-ferromagnetic below ~33 K.[7] The crystal and magnetic structures of $CoGeO_3$ have previously been studied in detail,[7] and, below the Néel temperature, the first magnetic peak is known to be the strongest peak in the neutron diffraction pattern. In the absence of this peak, the impurity phase had not been detected in the diffraction data, X-ray or neutron, collected at 300 K. Nor was it detectable in the temperature dependence of the magnetic susceptibility. Using multiphase refinements to include CeO_2 and $CoGeO_3$ when appropriate, we were able to analyze successfully all the data sets collected. The patterns collected at 300 K for $x = 1.0$ and 1.5 were reanalyzed to determine the concentrations of the impurities,

DOI: 10.1021/acs.inorgchem.6b02905
Inorg. Chem. XXXX, XXX, XXX–XXX

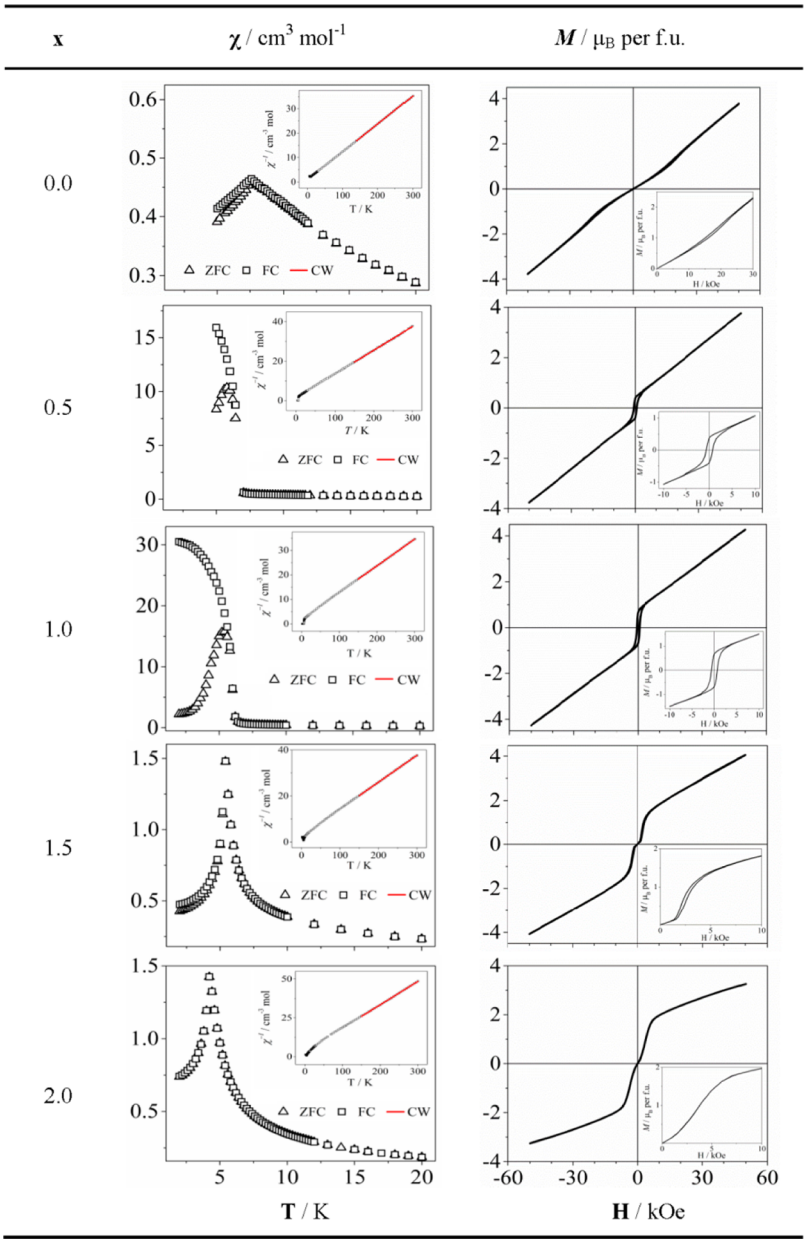

Figure 3. Temperature dependence of the dc molar magnetic susceptibility, measured in 100 Oe, and the field dependence of the magnetization at 2 K of $CeMn_{2-x}Co_xGe_4O_{12}$. (inset) The inverse susceptibility; data points highlighted in red were fitted to the Curie–Weiss law.

Table 1. Magnetic Parameters of $CeMn_{2-x}Co_xGe_4O_{12}$

	x				
	0.0	0.5	1.0	1.5	2.0
C, cm³ K mol⁻¹	8.745(1)	8.344(4)	7.943(1)	7.586(1)	7.186(2)
θ, K	−7.59(3)	−13.06(8)	−17.50(2)	−21.96(2)	−15.93(2)
μ_{eff}^{Co}[a]	5.91[b]	5.36	5.35	5.37	5.36
T_c[c] K	7.6	6.5	5.8	5.4	4.2
M_r, μ_B per formula unit		0.38	0.67		
H_c, Oe		688	626		

[a]Calculated assuming μ_{eff}^{Mn} = 5.91 for all compositions. [b]μ_{eff}^{Mn}. [c]Curie or Néel temperature for ferromagnetic and anti-ferromagnetic compositions, respectively.

which were then held constant during the analysis of the data collected at 1.6 K. None of the low-temperature diffraction patterns showed any evidence that a structural phase transition had occurred on cooling the sample. The atomic coordinates and bond lengths at 300 and 1.6 K are listed for all compositions in Tables 2, 3, 4, and 5. The values reported at 1.6 K result from refinements in which the crystal and magnetic structures were refined simultaneously. The magnetic structure

DOI: 10.1021/acs.inorgchem.6b02905
Inorg. Chem. XXXX, XXX, XXX−XXX

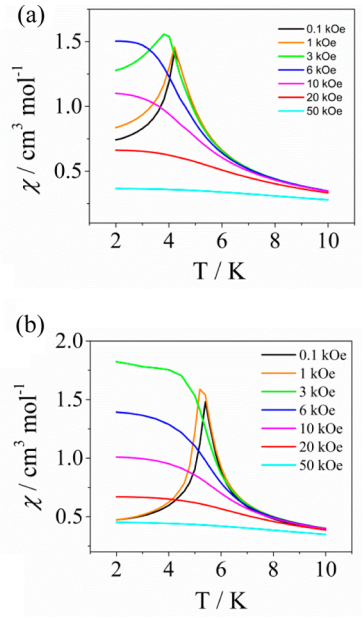

Figure 4. Temperature and field dependence of the dc molar magnetic susceptibility of (a) $CeMn_{0.5}Co_{1.5}Ge_4O_{12}$ and (b) $CeCo_2Ge_4O_{12}$.

of $CeMn_{2-x}Co_xGe_4O_{12}$ changes markedly as the composition varies; see Figure 8.[29] In Co-free $CeMn_2Ge_4O_{12}$, the magnetic moments of nearest-neighbor (NN) Mn^{2+} cations within the (001) sheet at $z = 1/2$ couple anti-ferromagnetically and align along [001]; the moments of next-nearest-neighbor (NNN) cations within this sheet align in a ferromagnetic manner, and the resulting structure is anti-ferromagnetic and can be described in the magnetic space group $P4'/nbm'$ (No. 125.5.1035); the structural and magnetic unit cells are the same size. The replacement of 25% of the Mn^{2+} cations by Co^{2+} causes the spins to rotate into the (001) plane, but, within the resolution of our data, the same collinear coupling scheme is retained. This magnetic structure, space group $Pb'an'$, No. 50.6.382, was also found to account for the diffraction data collected from $CeMnCoGe_4O_{12}$. However, when the Co^{2+} concentration was increased to 75% a different magnetic structure was observed. The unit cell doubles along [001], and the NN coupling in this direction changes from ferromagnetic to anti-ferromagnetic. Within the (001) sheets, the coupling scheme described above is retained along one axis, but the components perpendicular to that axis align in a ferromagnetic manner. The magnetic structure can thus be described as an anti-ferromagnetic stacking of weakly ferromagnetic sheets in space group $P_{2_c}b'an$, No. 50.9.385. This magnetic structure is also adopted by the manganese-free end member, $CeCo_2Ge_4O_{12}$. The values of the refined components, M_i, of the magnetic moments, their resultant, M_T, and the angles between M_T and the long axis of the Mn/CoO_6 octahedra are compiled in Table 6; a fitted diffraction pattern representative of each of the three observed magnetic structures is shown in Figure 9.

In the light of the relatively unusual magnetometry data shown in Figures 3−5, further neutron diffraction data were collected at 1.6 K in an applied magnetic field using a wavelength λ = 2.4395 Å. The values of the refined magnetic moments in a field of 20 kOe are included in Table 6. The very weak dependence of the unit-cell parameters on the field strength is illustrated in Figure 10. The magnetic structure of $CeMn_2Ge_4O_{12}$ did not change on the application of a magnetic field. However, there was a significant reduction in the magnitude of the ordered magnetic moment, as is shown by the decrease in intensity apparent in all the reflections with a magnetic contribution, see Figure 11. This effect was reversible. The in-field data collected on the samples having x = 0.5, 1.0 were fitted using the same model as was used to account for the zero-field data from the same compositions. The agreement between the observed and calculated diffraction patterns could be described as acceptable, as exemplified by Figure 12a, and no significant field dependence of the ordered moment was observed in these two compositions. However, we are unable to explain why the intensity of just one reflection, the 310, is reduced when a field is applied. Furthermore, the change is irreversible. To restore the intensity of this reflection it was necessary to switch off the field, warm the sample above the transition temperature, and then recool to 1.6 K; see Figure 12b. The magnetic structures of $CeMn_{0.5}Co_{1.5}Ge_4O_{12}$ and $CeCo_2Ge_4O_{12}$ did show a marked change when a field of 20 kOe was applied. More specifically, although the noncollinear spin arrangement was retained, the unit cell doubling observed at low temperatures in zero field was lost, leading to a change from anti-ferromagnetism to weak ferromagnetism. The diffraction patterns collected in zero field and in 20 kOe are compared in Figure 13a,b, and the high-field structure is drawn in Figure 14. Patterns collected in intermediate fields could be fitted (see Figure 13c) by assuming that the two extreme structures coexist for $2 \le H \le 10$ kOe in the case of $CeCo_2Ge_4O_{12}$ and $2 \le H < 10$ kOe in the case of $CeCo_{1.5}Mn_{0.5}Ge_4O_{12}$. The relative proportions of the two phases were refined (see Table 7) with the assumption that each had the same ordered cation moment as when it was the only phase present.

DISCUSSION

$CeMn_2Ge_4O_{12}$ and $CeCo_2Ge_4O_{12}$ form a solid solution for all values of the ratio Mn/Co, and there is no significant structural change on cooling from room temperature to 1.6 K; see Tables 3 and 5. The bond lengths in $CeMn_2Ge_4O_{12}$ at room temperature are consistent with those reported previously.[17] We note that, in contrast to $Y_2CoGe_4O_{12}$,[25] there was no evidence for disorder on the oxide sublattices in $CeMn_{2-x}Co_xGe_4O_{12}$. The yttrium-containing compound has a disordered distribution of Y^{3+} and Co^{2+} over the 4f sites, and it seems likely that this cation disorder is responsible for the observed anion disorder. The unit cell parameters in the Ce-based solid solution decrease as the cobalt content increases from x = 0 to x = 2, a by 0.96% and c by 1.81%; the ratio a/c consequently increases from 2.004 to 2.021. This is consistent with the difference in size between Mn^{2+} and Co^{2+}.[30] The only bond lengths to show a systematic and significant change as a function of composition are those within the $(Mn/Co)O_6$ octahedra; see Table 3. The pseudotetragonal strain in these octahedra, defined as $((Mn/Co-O)_{eq}-(Mn/Co-O)_{ax})/(Mn/Co-O)_{eq}$, varies from −0.141 to −0.149 across the series. The Mn^{2+} and Co^{2+} cations occupy a site with point symmetry 2/m, and the oxide ions to which they are coordinated therefore do not form a regular octahedron. In each case there are two long, *trans* bonds to O1 (see Tables 3 and 5) and four shorter, coplanar bonds to O2; the plane in which the latter lie is not exactly perpendicular to the axis formed by the long bonds. The mean bond lengths in the MnO_6 and CoO_6 octahedra of the compositions x = 0.0 and 2.0 are 2.234 and 2.168 Å, respectively; the corresponding values in MnO and CoO are 2.223 and 2.132 Å at room temperature.[31] The four O2 anions that coordinate the cation in the plane form a rectangle rather than a square, with O2−O2 distances of 3.220 and 2.790 Å at 1.6 K in the Mn-containing compound and

DOI: 10.1021/acs.inorgchem.6b02905
Inorg. Chem. XXXX, XXX, XXX−XXX

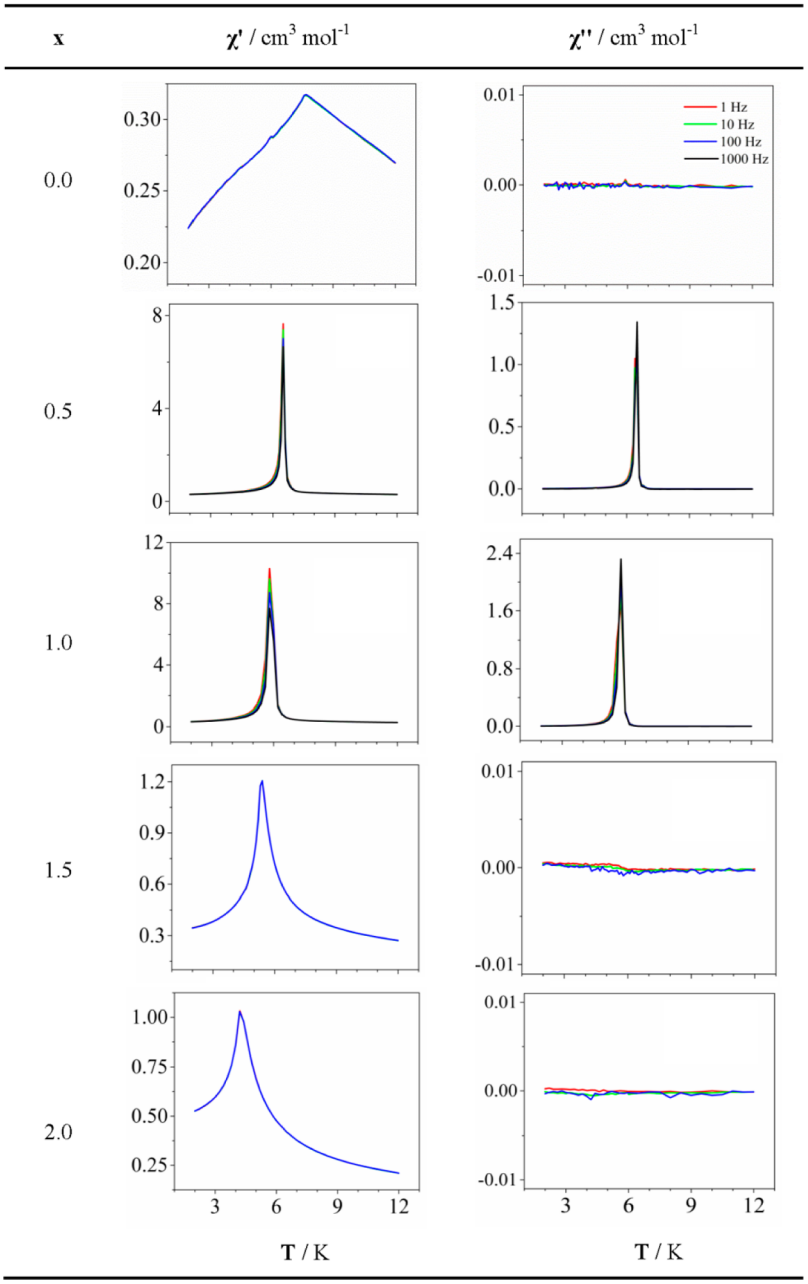

Figure 5. Temperature and frequency dependence of the ac molar magnetic susceptibility of $CeMn_{2-x}Co_xGe_4O_{12}$.

3.114 and 2.699 Å at 1.6 K in $CeCo_2Ge_4O_{12}$. The Ce−O distances within the square antiprism of oxide ions that surround the 2b site in $CeMn_2Ge_4O_{12}$ and $CeCo_2Ge_4O_{12}$ are very similar to each other and also to the value of 2.343 Å determined for eight-coordinate Ce^{4+} in cubic CeO_2.[32] The O−O distances within the square faces of the antiprism are 2.834 Å in $CeCo_2Ge_4O_{12}$; the distances between anions in the opposing faces are alternately 2.903 and 2.699 Å; that is, the CoO_6 octahedra share their trans short edges with neighboring CeO_8 antiprisms. For comparison, the O−O distance in CeO_2 is 2.706 Å, similar to the shortest O−O contact in the germanate. The GeO_4 tetrahedra in both $CeMn_2Ge_4O_{12}$ and $CeCo_2Ge_4O_{12}$ show a considerable degree of distortion, as was also the case in $Y_2CoGe_4O_{12}$. The longer Ge−O1 bonds provide the connectivity between the four GeO_4 tetrahedra that make up a Ge_4O_{12} group, whereas each O2 atom is bonded to only one germanium atom.

Unlike the crystal structure, the magnetic properties show a wide variation with composition, although the negative Weiss temperatures listed in Table 1 indicate that anti-ferromagnetic interactions are dominant in every composition. The effective magnetic moment of Mn^{2+} derived from the paramagnetic Curie constant of $CeMn_2Ge_4O_{12}$, 5.91 μ_B, is in good agreement with the value of 5.92 μ_B predicted by the spin-only formula. Table 1 lists the effective magnetic moment of Co^{2+} in each composition, assuming that the moment of Mn^{2+} is constant across the series. The derived values do not differ significantly across the series, and they are all larger than the spin-only moment, 3.87 μ_B, of a d^7 cation, although they are considerably lower than the value of 6.05 μ_B observed previously in $Y_2CoGe_4O_{12}$. There is clearly a considerable orbital contribution to the moment, despite the relatively low 2/*m* point symmetry of the 4f site. It was suggested[25] that the high moment observed

DOI: 10.1021/acs.inorgchem.6b02905
Inorg. Chem. XXXX, XXX, XXX−XXX

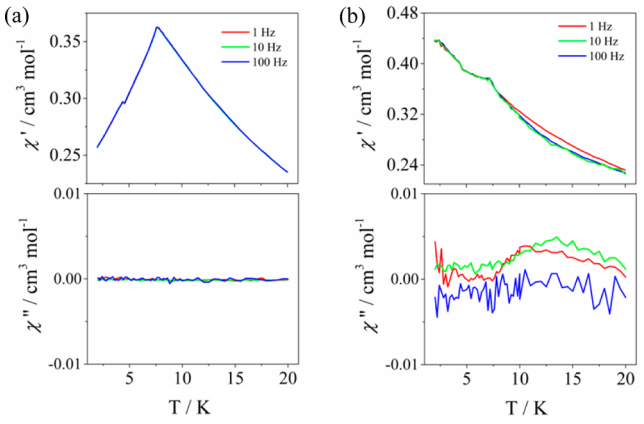

Figure 6. Temperature and frequency dependence of the ac molar magnetic susceptibility of $CeMn_2Ge_4O_{12}$ in dc fields of (a) 500 Oe and (b) 20 kOe.

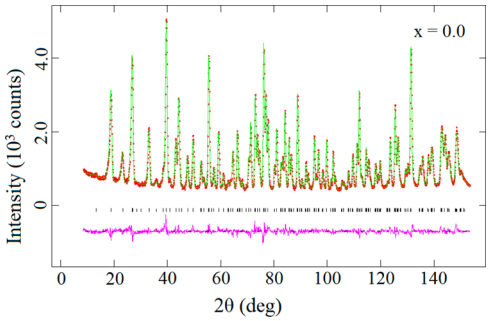

Figure 7. Observed (red dots) and calculated (green line) NPD patterns of $CeMn_2Ge_4O_{12}$ at room temperature; λ = 1.622 Å. A difference curve (purple line) is shown, and reflection positions are marked.

in $Y_2CoGe_4O_{12}$ was a consequence of the high value, −0.173, of the strain parameter defined above, and, consistent with that proposal, the lowering of the moment in the present study is accompanied by a decrease in the strain parameter.

The ac susceptibility of $CeMn_{2.0}Ge_4O_{12}$ (see Figure 5) suggests that the compound is anti-ferromagnetic in the absence of an applied field. However, the dc susceptibility, measured in 100 Oe, shows clear evidence of FC/ZFC hysteresis, and $M(H)$ is nonlinear and shows weak hysteresis when $10 < H < 25$ kOe; see Figure 3. The magnetic structure determined by neutron diffraction in zero field is anti-ferromagnetic with an ordered moment of 4.61(2) μ_B per Mn^{2+} cation. This value is the same as that in MnO;[33] the reduction from the saturation value $gS = 5$ μ_B is attributable to the covalency in the Mn−O bonds. The magnitude of the ordered moment decreases when a field is applied, and we therefore conclude that this composition is a collinear-spin anti-ferromagnet in zero field but that partial spin disorder is induced by the application of an external field of 100 Oe or more. The nature of the spin disorder is not clear; the ac susceptibility measured in dc fields of 500 and 2×10^4 Oe (see Figure 6) is real, but the data collected in the higher field show an apparently paramagnetic component below T_N. We suggest that the disordered spin components lie in the (001) planes, but this is speculation at the present time.

The replacement of 25% of the Mn^{2+} cations by Co^{2+} is enough to cause a major change in the magnetic behavior in zero field, with the ordered magnetic moments lying in the (001) plane rather than along the [001] axis. Furthermore, $\chi(T)_{dc}$, $\chi(T)_{ac}$, and $M(H)$ are all consistent with the formation of a weakly ferromagnetic phase, that is, a canted anti-ferromagnet, at low temperatures. The ferromagnetic component of the mean ordered atomic moment was too small to be detected by neutron diffraction, but such a component is allowed in the magnetic space group *Pb′an′*. This was to be expected in view of the low value of the remanent magnetization measured by magnetometry. The measured value of the zero-field ordered moment is significantly smaller than that of $CeMn_{2.0}Ge_4O_{12}$. Some reduction is to be expected as Mn^{2+}:d^5 is replaced by Co^{2+}:d^7, but if the moment of the former is assumed to be constant then the ordered moment of the latter is only ∼1.85 μ_B, well below the spin-only value of 3 μ_B. We recognize that there is a weak ferromagnetic component that we could not detect in our neutron data, but our magnetometry data (see Table 1)

Table 2. Structural Parameters[a] of $CeMn_{2-x}Co_xGe_4O_{12}$ at Room Temperature Derived from Neutron Diffraction Data

		x				
		0.0	0.5	1.0[b]	1.5[c]	2.0
Ce[d]	U_{iso}, Å²	0.0037(8)	0.0040(7)	0.0084(7)	0.0085(8)	0.0031(8)
Mn/Co	U_{iso}, Å²	0.0070(5)	0.0107(9)	0.0144(6)	0.0242(2)	0.0052(1)
Ge	x	0.5233(1)	0.5240(1)	0.5232(2)	0.5234(2)	0.5242(1)
	U_{iso}, Å²	0.0025(2)	0.0040(2)	0.0078(4)	0.0081(6)	0.0031(2)
O1	x	−0.3694(1)	−0.3692(1)	−0.3692(2)	−0.3691(2)	−0.3689(1)
	z	0.1697(3)	0.1728(3)	0.1754(5)	0.1778(5)	0.1803(3)
	U_{iso}, Å²	0.0040(3)	0.0062(3)	0.0109(8)	0.0110(7)	0.0053(4)
O2	x	0.1672(1)	0.1660(1)	0.1646(2)	0.1636(2)	0.1621(1)
	y	0.0646(1)	0.0645(1)	0.0644(2)	0.0640(2)	0.0640(1)
	z	0.2551(2)	0.2560(2)	0.2550(4)	0.2542(4)	0.2561(3)
	U_{iso}, Å²	0.0044(2)	0.0065(2)	0.0094(5)	0.0091(5)	0.0058(3)
a, Å		9.8382(1)	9.8130(1)	9.7925(2)	9.7695(2)	9.7434(1)
c, Å		4.9096(1)	4.8861(1)	4.8640(1)	4.8423(2)	4.8207(1)
V, Å³		475.20(1)	470.52(1)	466.42(3)	462.10(3)	457.65(2)
R_{wpr}		4.74%	4.48%	5.81%	6.06%	4.80%
χ^2		2.206	2.439	2.090	2.276	2.432

[a]Space group *P4/nbm* (No. 125), Z = 2; λ = 1.622 Å. [b]Contains 1.3(2) wt % $CoGeO_3$ and 0.3(1) wt % CeO_2. [c]Contains 4.1(6) wt % $CoGeO_3$ and 0.9(1) wt % CeO_2. [d]Ce on 2b (1/4, 1/4, 1/2); Mn/Co on 4f (0, 0, 1/2); Ge on 8k (x, 1/4, 0); O1 on 8m (x, −x, z); O2 on 16n (x, y, z).

DOI: 10.1021/acs.inorgchem.6b02905
Inorg. Chem. XXXX, XXX, XXX−XXX

Table 3. Bond Lengths (Å) and Bond Angles (degrees) in $CeMn_{2-x}Co_xGe_4O_{12}$ at Room Temperature

	x				
	0.0	0.5	1.0	1.5	2.0
Ce−O2 × 8	2.331(1)	2.327(1)	2.329(2)	2.331(2)	2.324(1)
Mn/Co−O1 × 2	2.435(1)	2.419(1)	2.402(3)	2.388(3)	2.374(2)
Mn/Co−O2 × 4	2.134(1)	2.116(1)	2.102(2)	2.088(2)	2.066(1)
O2−O2′[a]	3.225(1)	3.199(1)	3.172(3)	3.143(3)	3.116(2)
O2−O2″[a]	2.796(1)	2.770(1)	2.758(3)	2.750(3)	2.712(2)
Ge−O1 × 2	1.786(1)	1.783(1)	1.789(1)	1.789(2)	1.784(1)
Ge−O2 × 2	1.727(1)	1.731(1)	1.725(2)	1.719(2)	1.731(1)
O2−Mn/Co−O2′	98.16(4)	98.22(4)	97.98(7)	97.65(7)	97.92(5)
O2−Mn/Co−O2″	81.84(4)	81.78(4)	82.02(7)	82.35(7)	82.01(5)
O1−Mn/Co−O2′	82.77(4)	82.96(4)	82.90(8)	82.94(8)	83.09(5)
O1−Mn/Co−O2″	97.23(4)	97.04(4)	97.10(8)	97.06(8)	96.92(5)
O1−Ge−O1	107.57(11)	108.04(10)	107.90(21)	108.05(22)	108.58(13)
O1−Ge−O2	105.56(5)	105.36(5)	105.43(9)	105.44(10)	105.27(6)
O1−Ge−O2	108.91(7)	108.94(6)	108.64(13)	108.46(13)	108.42(8)
O2−Ge−O2	119.84(8)	119.78(8)	120.31(15)	120.51(16)	120.48(10)

[a]Distances within the equatorial plane of the $(Mn/Co)O_6$ octahedra.

Table 4. Structural Parameters[a] of $CeMn_{2-x}Co_xGe_4O_{12}$ at 1.6 K Derived from Neutron Diffraction Data

		x				
		0.0	0.5	1.0	1.5	2.0
Ce[b]	U_{iso}, Å^2	0.0016(5)	0.0010(2)	0.0051(5)	0.0063(3)	0.0048(3)
Mn/Co	U_{iso}, Å^2	0.0017(3)	0.0064(3)	0.0033(3)	0.0196(6)	0.0020(4)
Ge	x	0.5234(1)	0.5240(1)	0.5232(2)	0.5231(2)	0.5244(1)
	U_{iso}, Å^2	0.0008(2)	0.0006(1)	0.0044(4)	0.0046(4)	0.0016(2)
O1	x	−0.3698(1)	−0.3696(1)	−0.3686(2)	−0.3690(2)	−0.3690(1)
	z	0.1710(2)	0.1730(2)	0.1753(4)	0.1787(5)	0.1806(2)
	U_{iso}, Å^2	0.0014(2)	0.0020(2)	0.0048(5)	0.0061(6)	0.0040(3)
O2	x	0.1669(1)	0.1655(1)	0.1646(2)	0.1633(2)	0.1619(1)
	y	0.0647(1)	0.0645(1)	0.0643(2)	0.0644(2)	0.0642(1)
	z	0.2550(2)	0.2556(2)	0.2542(4)	0.2544(4)	0.2569(2)
	U_{iso}, Å^2	0.0025(2)	0.0029(2)	0.0046(2)	0.0050(3)	0.0039(4)
a, Å		9.8317(1)	9.8080(1)	9.7892(2)	9.7668(1)	9.7369(1)
c, Å		4.9024(1)	4.8794(1)	4.8570(1)	4.8356(1)	4.8126(1)
V, Å^3		473.878(1))	469.387(1))	465.444(12)	461.270(12)	456.268(11)
R_{wpr}		4.20%	4.49%	6.52%	6.38%	3.62%
χ^2		4.570	2.322	2.418	2.601	3.392

[a]Space group $P4/nbm$ (No. 125), Z = 2; λ = 1.622 Å. [b]Ce on 2b (1/4, 1/4, 1/2); Mn/Co on 4f (0, 0, 1/2); Ge on 8k (x, 1/4, 0); O1 on 8m (x, $-x$, z); O2 on 16n (x, y, z).

Table 5. Bond Lengths (Å) and Bond Angles (degrees) in $CeMn_{2-x}Co_xGe_4O_{12}$ at 1.6 K

	x				
	0.0	0.5	1.0	1.5	2.0
Ce−O2 × 8	2.330(1)	2.328(1)	2.330(2)	2.327(2)	2.320(1)
Mn/Co−O1 × 2	2.425(1)	2.411(1)	2.408(3)	2.385(3)	2.370(1)
Mn/Co−O2 × 4	2.131(1)	2.111(1)	2.102(2)	2.085(2)	2.060(1)
O2−O2′[a]	3.220(1)	3.190(1)	3.169(3)	3.143(3)	3.114(1)
O2−O2″[a]	2.790(1)	2.766(1)	2.762(3)	2.741(3)	2.699(2)
Ge−O1 × 2	1.786(1)	1.783(1)	1.787(2)	1.791(2)	1.782(1)
Ge−O2 × 2	1.727(1)	1.731(1)	1.719(2)	1.721(2)	1.734(1)
O2−Mn/Co−O2′	98.19(3)	98.13(3)	97.84(7)	97.82(7)	98.16(3)
O2−Mn/Co−O2″	81.81(3)	81.87(3)	82.16(7)	82.18(7)	81.84(3)
O1−Mn/Co−O2′	82.75(3)	82.82(3)	82.98(7)	82.93(7)	83.12(3)
O1−Mn/Co−O2″	97.25(3)	97.18(3)	97.02(7)	97.07(7)	96.88(3)
O1−Ge−O1	108.04(8)	108.37(9)	107.28(20)	107.95(20)	108.71(8)
O1−Ge−O2	105.50(4)	105.51(4)	105.60(9)	105.47(9)	105.29(4)
O1−Ge−O2	108.82(5)	108.63(6)	108.76(12)	108.50(12)	108.43(5)
O2−Ge−O2	119.73(6)	119.82(7)	120.26(15)	120.47(15)	120.33(6)

[a]Distances within the equatorial plane of the $(Mn/Co)O_6$ octahedra.

DOI: 10.1021/acs.inorgchem.6b02905
Inorg. Chem. XXXX, XXX, XXX−XXX

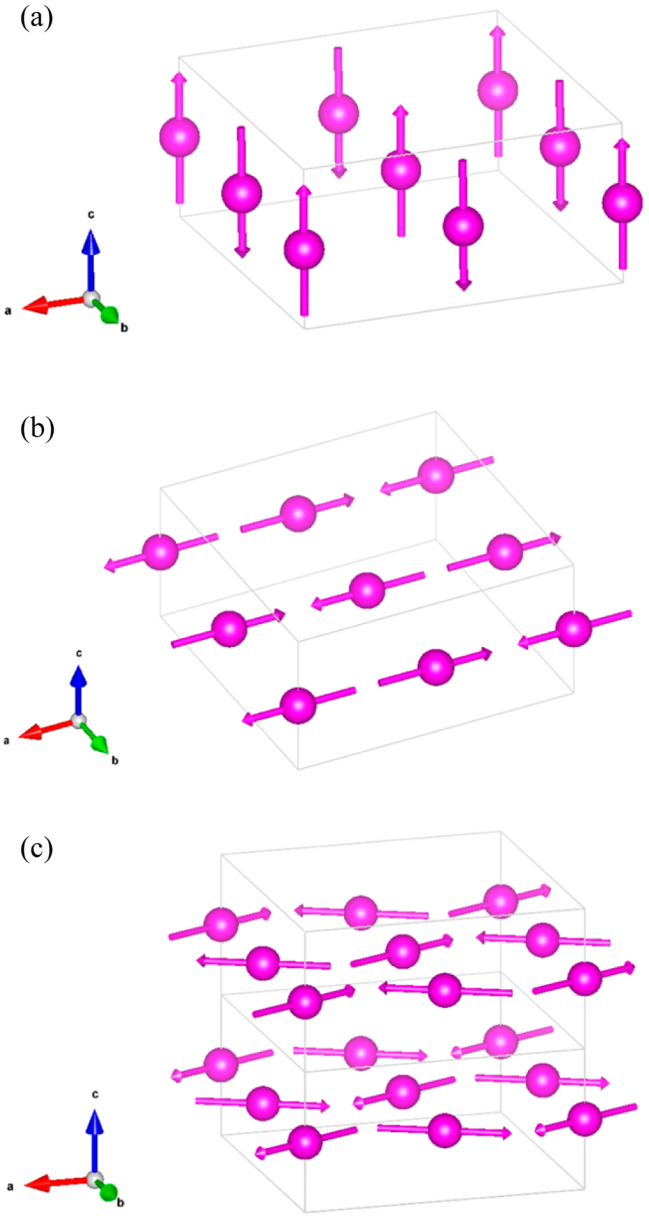

Figure 8. Magnetic structure in zero field of $CeMn_{2-x}Co_xGe_4O_{12}$ with x = (a) 0.0, (b) 0.5 and 1.0, and (c) 1.5 and 2.0. Diamagnetic ions are omitted.

identified a remanent magnetization of only 0.38 μ_B per formula unit, which is not large enough to carry the moment into the expected range. The presence of a large orbital contribution to the effective moment in the paramagnetic phase makes the low value of the ordered moment even more noteworthy. The replacement of a further 25% of Mn^{2+} by Co^{2+} has no major effect on the magnetic properties; the value of the ordered moment per cation decreases further, and at low temperature the compound is a canted anti-ferromagnet with a resultant magnetization that is again too weak to be detected by neutron diffraction. The ordered moment calculated for the Co^{2+} cations using the assumptions described above, ~1.7 μ_B, is again surprisingly small. One interpretation of these data is that not all the atomic moments take part in the long-range magnetic ordering. The ac susceptibility data presented in Figure 5 show no evidence for the coexistence of a glassy phase with the ordered phase, but we cannot rule out the possibility that some spins remain paramagnetic.

Table 6. Mean Ordered Atomic Moments (μ_B) at the 4f Site in $CeMn_{2-x}Co_xGe_4O_{12}$ as a Function of Applied Magnetic Field and Composition at 1.6 K

		x				
H, kOe		0.0	0.5[a]	1.0	1.5	2.0
0	M_x	0	3.92(2)	3.13(4)	2.68(3)	2.29(2)
	M_y[b]	0	0	0	0.91(6)	1.19(3)
	M_z	4.61(2)	0	0	0	0
	M_T	4.61(2)	3.92(2)	3.13(4)	2.83(3)	2.58(2)
	φ[c]	48.30(1)	58.00(1)	52.06(2)	69.1(1)	72.5(2)
20	M_x	0	3.84(2)	3.17(4)	2.72(4)	2.41(3)
	M_y[b]	0	0	0	1.43(12)	1.85(5)
	M_z	4.34(2)	0	0	0	0
	M_T	4.34(2)	3.84(2)	3.17(4)	3.07(7)	3.04(4)

[a]For x = 0.5, the data refer to fields of 0 kOe and 10 kOe. [b]The ferromagnetic component. [c]The angle between M_T and the long axis of the Mn/CoO_6 octahedra at 1.6 K.

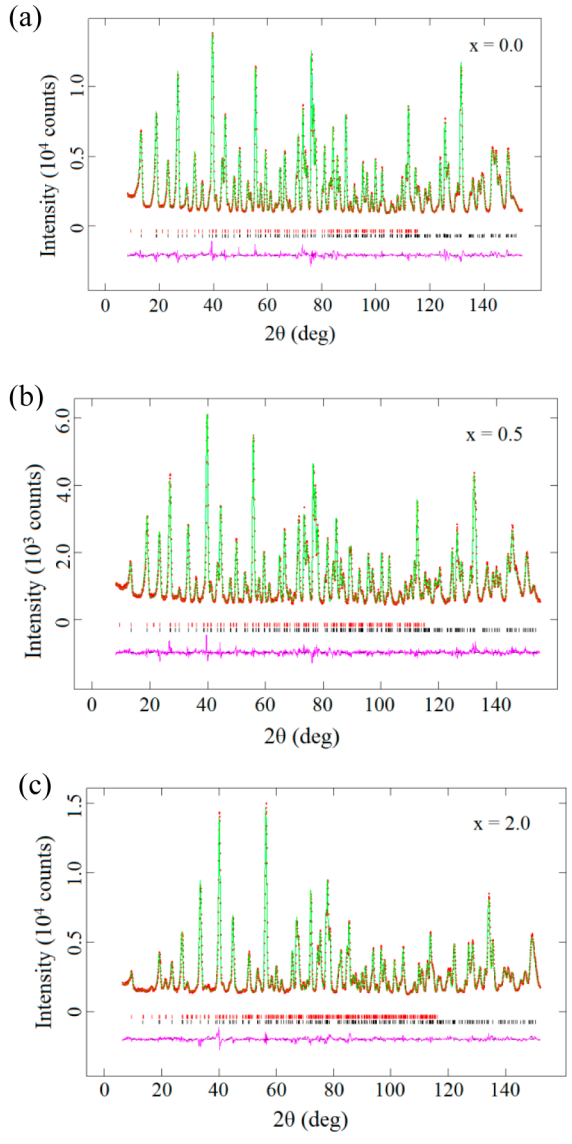

Figure 9. Observed (red dots) and calculated (green line) NPD patterns of $CeMn_{2-x}Co_xGe_4O_{12}$ for x = (a) 0.0, (b) 0.5, (c) 2.0 at 3 K, λ = 1.622 Å. A difference curve (purple line) is shown, and reflection positions are marked.

DOI: 10.1021/acs.inorgchem.6b02905
Inorg. Chem. XXXX, XXX, XXX−XXX

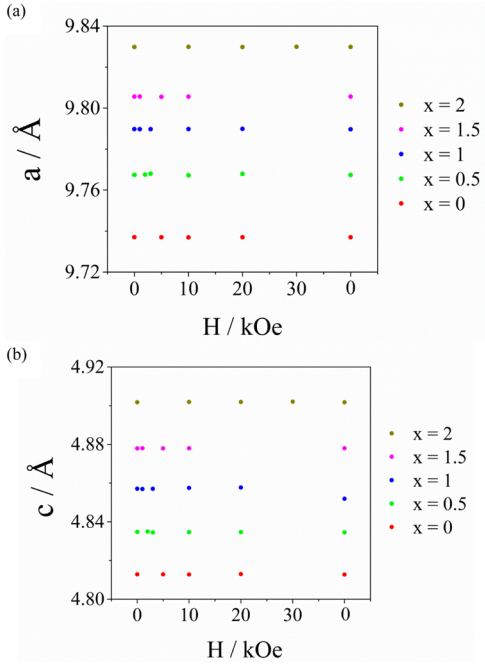

Figure 10. Dependence of the unit cell parameters (a) a and (b) c on composition and applied magnetic field at 1.6 K. The field was increased to the maximum value and then returned to zero.

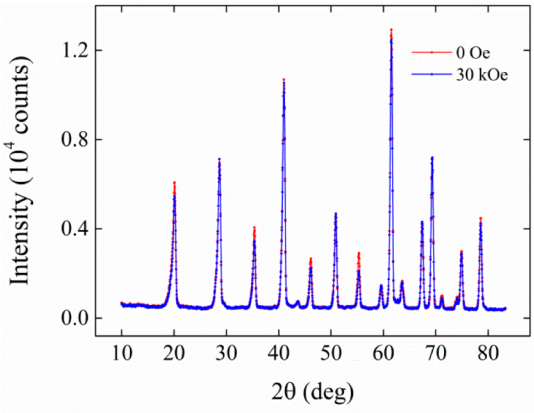

Figure 11. Low-angle region of the neutron diffraction pattern of $CeMn_2Ge_4O_{12}$ in applied fields of 0 (blue) and 30 (red) kOe at 1.6 K, λ = 2.4395 Å.

The behavior of $CeMn_{0.5}Co_{1.5}Ge_4O_{12}$ is very different to that of the compositions described above. The ac susceptibility (see Figure 5) shows it to be an anti-ferromagnet in zero field, and the dc susceptibility shows that this behavior is maintained in 100 Oe; see Figure 3. However, $M(H)$ (see Figure 3) indicates that the application of higher fields disrupts this state, and $\chi(T)_{dc}$ measured in higher fields (see Figure 4a) shows that fields greater than 3 kOe change the nature of the ground state. Our neutron data reveal the details of the change. In zero field at 1.6 K this composition is indeed anti-ferromagnetic. The ordered spin structure is similar to that of the composition x = 1.0 in that it consists of weakly ferromagnetic sheets perpendicular to [001]. However, in the more Co-rich composition the sheets stack anti-ferromagnetically, thus doubling the periodicity of the unit cell and canceling the weak ferromagnetism. When a magnetic field is applied, the doubling is lost, and the structure transforms to that of the weak ferromagnet shown

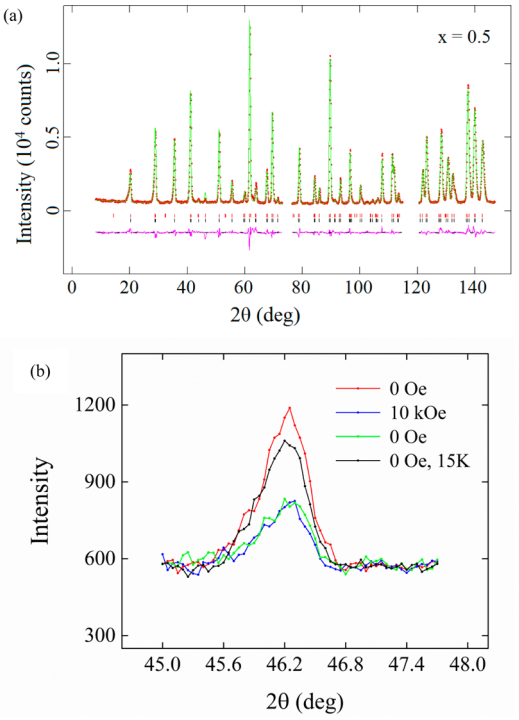

Figure 12. (a) Observed (red dots) and calculated (green line) NPD patterns of $CeMn_{1.5}Co_{0.5}Ge_4O_{12}$ in a field of 20 kOe at 1.6 K, λ = 2.4395 Å. A difference curve (purple line) is shown, and reflection positions are marked; (b) the 310 reflection before (red), during (blue) and after (green) the application of a 10 kOe field. The black curve was recorded after heating the sample to 15 K and recooling to 1.6 K.

in Figure 14. The data in Figures 3e, 4e, 5b, 6e, and 14 demonstrate that the Mn-free end member, $CeCo_{2.0}Ge_4O_{12}$, behaves in a similar manner. This composition gives an unambiguous value of 2.58(2) μ_B for the ordered moment of Co^{2+} in zero field at low temperatures. This is in the range that would be expected for an S = 3/2 cation with no orbital contribution to the moment. Our data thus suggest that the Co^{2+} cations have an orbital contribution to their angular momentum in the high-temperature, paramagnetic phase but that this component is absent from the low-temperature, magnetically ordered phase. We shall return to this point below.

To rationalize the magnetic structures adopted and the changes therein as a function of composition it is necessary to consider the superexchange pathways that operate within the crystal structure. The magnetic coupling between pairs of d^5 and d^7 cations is expected to be anti-ferromagnetic. Each cation within the layer at z = 1/2 has four nearest-neighbor (NN_i) cations in the layer at a distance $a/2$ and four next-nearest-neighbor (NNN_i) cations at a distance $\sqrt{2}a/2$; the subscripts i and o will be used to distinguish neighbors within and out of a single layer. Each pair of NN_i cations are linked via two Mn/Co−O1−Ge−O2−Mn/Co superexchange pathways involving germanate groups lying both above and below the z = 1/2 layer; see Figure 15. No Mn/Co−O−Ge−O−Mn/Co superexchange pathways couple NNN_i cations. They are linked instead via Mn/Co−O2−Ce−O2−Mn/Co pathways, which are both longer and less covalent than those involving germanium. The NN_i superexchange is therefore expected to be stronger than that between NNN_i, and so the resulting in-plane ordering preferentially leaves each Mn/Co cation coupled anti-ferromagnetically to four NN_i cations and consequently

DOI: 10.1021/acs.inorgchem.6b02905
Inorg. Chem. XXXX, XXX, XXX−XXX

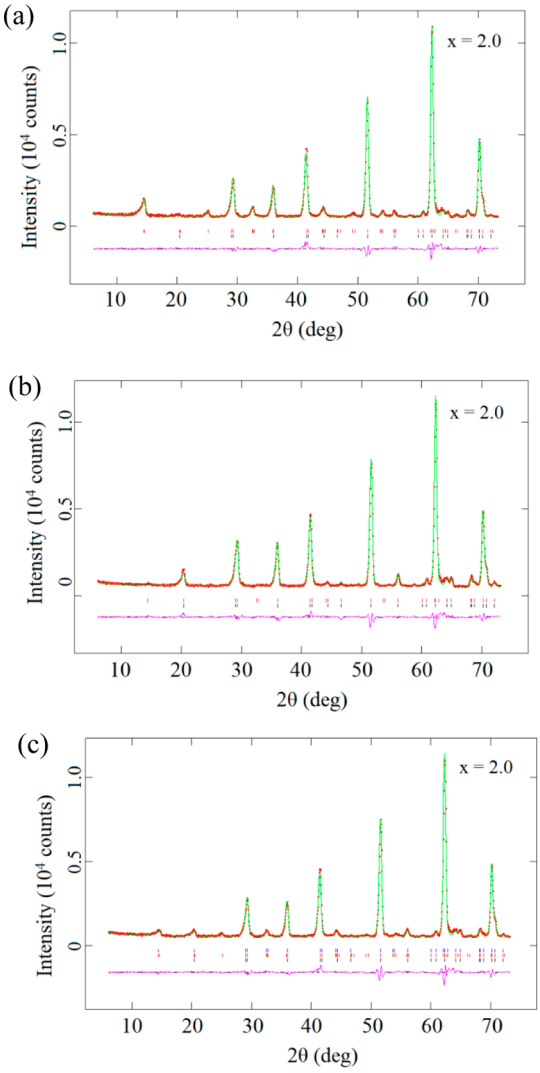

Figure 13. Observed (red dots) and calculated (green line) low-angle NPD patterns of $CeCo_{2.0}Ge_4O_{12}$ in fields of (a) 0, (b) 20, and (c) 5 kOe at 1.6 K, λ = 2.4395 Å. A difference curve (purple line) is shown, and reflection positions are marked.

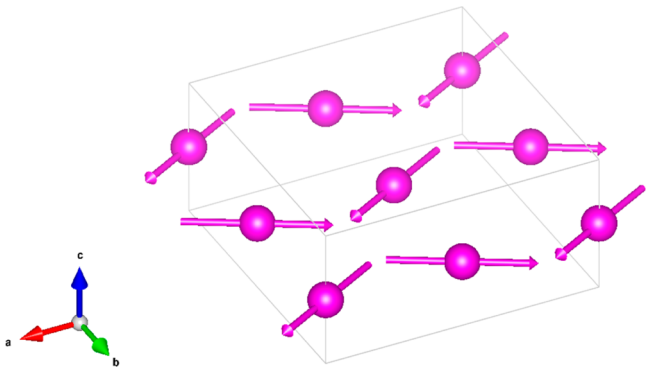

Figure 14. High-field magnetic unit cell of $CeCo_2Ge_4O_{12}$; only Co^{2+} cations are shown.

aligned ferromagnetically with four NNN_i cations. The interlayer coupling is less easy to predict, because both NN_o and NNN_o cations are linked by Mn/Co−O−Ge−O−Mn/Co pathways in this direction; see Figure 15. Each cation is coupled to both the cation immediately above it and that below it along

Table 7. Relative Phase Fractions of High-Field and Low-Field Phases Present in $CeMn_{2-x}Co_xGe_4O_{12}$ (x = 1.5, 2.0) at Intermediate Fields

x	H, kOe	% high-field phase	% low-field phase
1.5	2	19(1)	81(1)
	3	22(2)	78(2)
2.0	5	32.8(9)	67.2(9)
	10	90.2(6)	9.8(6)

[001] by four Mn/Co−O1−Ge−O2−Mn/Co superexchange pathways. It is also linked along ⟨101⟩ to four NNN_o cations in the plane above and four in the plane below. Of these eight pathways, four are of the form Mn/Co−O1−Ge−O1−Mn/Co, and the remainder are Mn/Co−O2−Ge−O2−Mn/Co pathways. The Mn/Co−O2 bonds are shorter than the Mn/Co−O1 bonds, and the O2−Ge−O2 bond angle is more open than the O1−Ge−O2 angle. It might therefore be expected that the Mn/Co−O2−Ge−O2−Mn/Co pathway between NNN_o provides the strongest anti-ferromagnetic superexchange interaction in the structure. The above discussion focuses on Mn/Co−O2−Ge−O2−Mn/Co pathways. Others have considered the interactions in comparable compounds in terms of simpler cation −O−O− cation pathways.[34,35] The O−O distances d, in the GeO_4 tetrahedra of $CeMn_{2-x}Co_xGe_4O_{12}$ (2.794 < d < 3.012 Å for x = 2), are too long for this interaction to dominate, and the involvement of the electron density in the bonds within the GeO_4 tetrahedra is likely to be crucial in establishing intercation coupling in this case.

The magnetic structure of $CeMn_2Ge_4O_{12}$ in the absence of an applied field (see Figure 8a) is consistent with this account; each spin is aligned antiparallel to four NN_i spins in the same (001) sheet and antiparallel to eight ⟨101⟩ NNN_o spins in the sheets above and below. The alignment of the spins along [001] minimizes dipolar repulsions within the structure. The magnetic structure of $CeMn_{2-x}Co_xGe_4O_{12}$; x = 0.5 and 1.0 (see Figure 8b), retains the underlying pattern of spin ordering, but the aligned spins now lie in the xy plane. The change in the preferred spin axis can be attributed to the asymmetric electronic ground state of Co^{2+}, which introduces an in-plane anisotropy that is strong enough, even at a concentration of 25%, to overcome the dipolar interactions. The spin−orbit coupling associated with the anisotropy is likely to be responsible for the weak ferromagnetism that could not be detected by neutron diffraction but which $M(H)$ shows to be present. The anti-ferromagnetic spin structure adopted by x = 1.5 and 2.0 in zero applied field also has the spins confined to the xy planes, but there is now anti-ferromagnetic alignment of NN_o along ⟨001⟩, causing a doubling of the unit cell parameter c. The loss of purely anti-ferromagnetic NN_i coupling and the consequent development of weak ferromagnetism within the xy planes can be deduced from the neutron data collected on these compositions; each of these planes has a net magnetization, the direction of which reverses between successive planes. The anti-ferromagnetic coupling between out-of-plane NNN_o cations, predicted on the basis of the bond lengths to be the strongest interaction, is also lost, although the alignment between third-nearest out-of-plane neighbors, separated by a vector 0.5**a** + 0.5**b** + **c**, changes from ferromagnetic to anti-ferromagnetic. We conclude that at high cobalt concentrations the energy of the system is minimized by the adoption of a structure different to that dictated by exchange energy alone. Detailed calculations are underway to understand this result better.

DOI: 10.1021/acs.inorgchem.6b02905
Inorg. Chem. XXXX, XXX, XXX−XXX

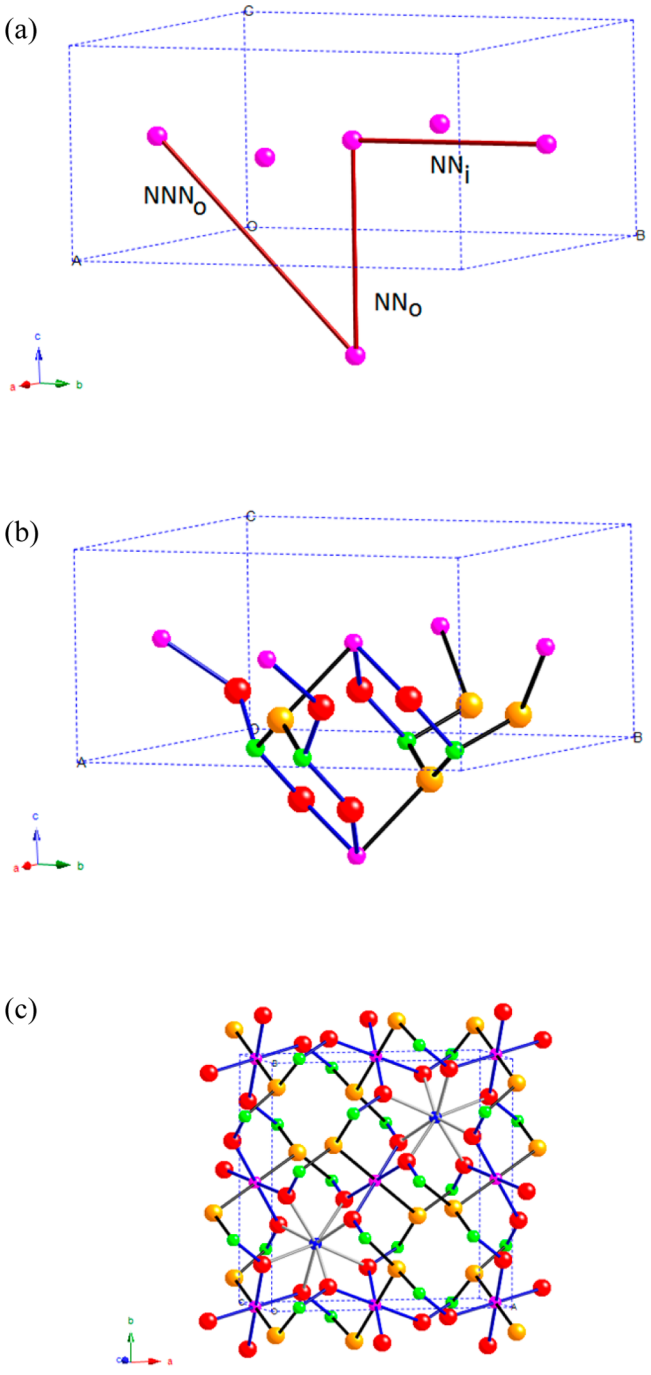

Figure 15. Structure of $CeMn_{2-x}Co_xGe_4O_{12}$ viewed to show (a) the principal superexchange interactions between magnetic cations and (b) an atomistic view of the principal superexchange pathways. Gold, red, green, and purple circles represent O1, O2, Ge, and Mn/Co, respectively. Bonds to O1 and O2 are black and blue, respectively. Two distinct NNN_o pathways can be seen. (c) The [001] view showing weak superexchange pathways involving Ce^{4+} cations (blue).

The behavior of $CeMn_2Ge_4O_{12}$ in an applied field was discussed above. We were unable to identify any changes in the magnetic structures of $CeMn_{1.5}Co_{0.5}Ge_4O_{12}$ and $CeMnCoGe_4O_{12}$ when a field was applied, and the behavior of $M(H)$ seen in Figure 4b,c is consistent with the weakly ferromagnetic structure identified in zero field. However, we emphasize that we cannot account for the field dependence of the intensity of the 310 reflection. The anti-ferromagnetic ordering of $CeMn_{0.5}Co_{1.5}Ge_4O_{12}$ and $CeCo_2Ge_4O_{12}$ identified by diffraction and magnetometry in fields of 0 and 100 Oe, respectively, is incompatible with the behavior of $M(H)$ at higher fields (see Figure 4d,e) and with the temperature dependence of the dc susceptibility in higher measuring fields (see Figure 4). Our in-field neutron diffraction experiments show that when $H \geq 10$ kOe the magnetic structure adopted by both compositions is similar to that adopted in zero field by the compositions having $x = 0.5$ and 1.5, but now the ferromagnetic component M_y is strong enough to be included in the analysis. This component is responsible for the behavior seen in the susceptibility data collected in high fields (see Figure 4). Data collected in the field range of $0 < H < 10$ kOe could be analyzed assuming that the sample contained a mixture of the weakly ferromagnetic high-field structure and the low-field structure, the former increasing in concentration with increasing field strength. This is consistent with the first-order phase transition indicated by $M(H)$ and most clearly illustrated for the composition $x = 1.5$ in Figure 3. The application of a field thus favors the phase with a spontaneous magnetization and a structure that is consistent with the predicted strengths of the exchange interactions. The ferromagnetic component of the cation moment deduced from the in-field NPD experiments is, unsurprisingly, slightly larger than the magnetization measured by magnetometry in comparable fields.

The magnetic properties of $CeMn_{2-x}Co_xGe_4O_{12}$ clearly vary markedly with both composition and applied field. The rotation of the spin axis between [001] and the xy plane as a function of composition is not surprising in view of the different anisotropies of Co^{2+} and Mn^{2+}. A similar change was observed between $Sr_2MnGe_2O_7$ and $Sr_2CoGe_2O_7$.[12] The observation of an orbital contribution to the magnetic moment of Co^{2+} in the paramagnetic phase but not in the ordered phase has also been seen previously.[12,36,37] The existence of such a contribution at low temperatures will depend on the relative magnitudes of k_BT, the noncubic component of the crystal-field splitting, the spin−orbit coupling constant, and the Zeeman splitting caused by the internal molecular field.[38] A spectroscopic investigation of $CeCo_2Ge_4O_{12}$ would provide valuable insight into this issue. We propose that the large pseudotetragonal strain and the overall $2/m$ symmetry at the 4f site play a key role in determining the magnetic properties. The application of a magnetic field reverses the direction of all the atomic moments in alternate xy layers of $CeCo_2Ge_4O_{12}$ and converts an anti-ferromagnet into a weak ferromagnet. Similar metamagnetic transitions have been reported previously in compounds of both Co^{2+} [39] and Mn^{2+}.[40] It would be interesting to study the phase diagram of a single crystal of $CeCo_2Ge_4O_{12}$ as a function of field and temperature below the zero-field Néel temperature.

CONCLUSIONS

The solid solution $CeMn_{2-x}Co_xGe_4O_{12}$ can be prepared for $0 \leq x \leq 2$. All compositions in the solution order magnetically at low temperature, $T_c < 8$ K, but the properties of the low-temperature phase vary with the Mn^{2+}/Co^{2+} ratio. When $x = 0.0$, the ground state is anti-ferromagnetic with the atomic moments aligned along [001]. The replacement of 25% Mn^{2+} by Co^{2+} is enough to rotate the spins into the (001) plane with the concomitant introduction of weak ferromagnetism. When the Co concentration is 75% or greater the magnetic unit cell doubles in size along [001], as weakly ferromagnetic (001) sheets stack anti-ferromagnetically. The application of an external field induces a first-order phase change to a weakly ferromagnetic

DOI: 10.1021/acs.inorgchem.6b02905
Inorg. Chem. XXXX, XXX, XXX−XXX

structure with a 50% smaller unit cell volume. The changes in magnetic behavior are thought to stem from the different anisotropies associated with Mn^{2+} and Co^{2+}, although the low point symmetry of the magnetic site, 2/*m*, makes detailed interpretation difficult without spectroscopic data. Magnetometry data recorded in the paramagnetic region show that the Co^{2+} cations have a large orbital contribution to their effective magnetic moment, but the atomic moment in the ordered phase is lower than the spin-only value.

AUTHOR INFORMATION

Corresponding Author

*E-mail: peter.battle@chem.ox.ac.uk.

ORCID

Maxim Avdeev: 0000-0003-2366-5809

Peter D. Battle: 0000-0003-0955-7676

Notes

The authors declare no competing financial interest.

REFERENCES

(1) Battle, P. D.; Cheetham, A. K.; Gleitzer, C.; Harrison, W. T. A.; Long, G. J.; Longworth, G. A novel magnetic phase-transition in anhydrous iron(III) phosphate, $FePO_4$. *J. Phys. C: Solid State Phys.* **1982**, *15*, L919−L924.

(2) Battle, P. D.; Cheetham, A. K.; Long, G. J.; Longworth, G. Study of the magnetic-properties of iron(III) molybdate, by susceptibility, Mossbauer, and neutron-diffraction techniques. *Inorg. Chem.* **1982**, *21*, 4223−4228.

(3) Long, G. J.; Longworth, G.; Battle, P.; Cheetham, A. K.; Thundathil, R. V.; Beveridge, D. Study of anhydrous iron(III) sulfate by magnetic-susceptibility, Mossbauer, and neutron-diffraction techniques. *Inorg. Chem.* **1979**, *18*, 624−632.

(4) Attfield, J. P.; Battle, P. D.; Cheetham, A. K.; Johnson, D. C. Magnetic structures and properties of alpha-$CrPO_4$ and alpha-$CrAsO_4$. *Inorg. Chem.* **1989**, *28*, 1207−1213.

(5) Neel, L. Proprietes magnetiques des ferrites - ferrimagnetisme et antiferromagnetisme. *Annales De Physique* **1948**, *3*, 137−198.

(6) Redhammer, G. J.; Roth, G.; Treutmann, W.; Hoelzel, M.; Paulus, W.; Andre, G.; Pietzonka, C.; Amthauer, G. The magnetic structure of clinopyroxene-type LiFeGe2O6 and revised data on multiferroic $LiFeSi_2O_6$. *J. Solid State Chem.* **2009**, *182*, 2374−2384.

(7) Redhammer, G. J.; Senyshyn, A.; Tippelt, G.; Pietzonka, C.; Roth, G.; Amthauer, G. Magnetic and nuclear structure and thermal expansion of orthorhombic and monoclinic polymorphs of CoGeO3 pyroxene. *Phys. Chem. Miner.* **2010**, *37*, 311−332.

(8) Redhammer, G. J.; Senyshyn, A.; Tippelt, G.; Pietzonka, C.; Treutmann, W.; Roth, G.; Amthauer, G. Magnetic and low-temperature structural behavior of clinopyroxene-type $FeGeO_3$: A neutron diffraction, magnetic susceptibility, and Fe-57 Mossbauer study. *Am. Mineral.* **2012**, *97*, 694−706.

(9) Redhammer, G. J.; Senyshyn, A.; Tippelt, G.; Roth, G. Magnetic spin structure of pyroxene-type $MnGeO_3$. *J. Phys.: Condens. Matter* **2011**, *23*, 254202.

(10) Redhammer, G. J.; Vorberg, C.; Tippelt, G. Crystal structure and high temperature phase relations of monoclinic and orthorhombic pyroxene-compounds $MnGeO_3$: a comparison. *Neues Jahrb. Mineral., Abh.* **2012**, *189*, 103−115.

(11) Solovyev, I. V. Magnetization-induced local electric dipoles and multiferroic properties of $Ba_2CoGe_2O_7$. *Phys. Rev. B: Condens. Matter Mater. Phys.* **2015**, *91*, 224423.

(12) Endo, T.; Doi, Y.; Hinatsu, Y.; Ohoyama, K. Magnetic and Neutron Diffraction Study on Melilite-Type Oxides $Sr_2MGe_2O_7$ (M = Mn, Co). *Inorg. Chem.* **2012**, *51*, 3572−3578.

(13) Hara, S.; Sato, H.; Narumi, Y. Exotic Magnetism of Novel S = 1 Kagome Lattice Antiferromagnet $KV_3Ge_2O_9$. *J. Phys. Soc. Jpn.* **2012**, *81*, 073707.

(14) Cascales, C.; Fernandez-Diaz, M. T.; Monge, M. A.; Bucio, L. Crystal structure and low-temperature magnetic ordering in rare earth iron germanates $RFeGe_2O_7$, R = Y, Pr, Dy, Tm, and Yb. *Chem. Mater.* **2002**, *14*, 1995−2003.

(15) Cascales, C.; Fernandez Diaz, M. T.; Monge, M. A. Low-temperature magnetic ordering in rare-earth copper germanates $R_2CuGe_4O_{12}$, R = Ho, Er. *Chem. Mater.* **2000**, *12*, 3369−3375.

(16) Cascales, C.; Monge, M. A. Crystal structure and influence of the rare-earth on the magnetic structure of copper germanates $R_2CuGe_4O_{12}$. *J. Alloys Compd.* **2002**, *344*, 379−384.

(17) Taviot-Gueho, C.; Leone, P.; Palvadeau, P.; Rouxel, J. CeMn2Ge4O12 and $GdMnGe_2O_7$. *J. Solid State Chem.* **1999**, *143*, 145−150.

(18) Leonidov, I. I.; Petrov, V. P.; Chernyshev, V. A.; Nikiforov, A. E.; Vovkotrub, E. G.; Tyutyunnik, A. P.; Zubkov, V. G. Structural and Vibrational Properties of the Ordered $Y_2CaGe_4O_{12}$ Germanate: A Periodic Ab Initio Study. *J. Phys. Chem. C* **2014**, *118*, 8090−8101.

(19) Leonidov, I. I.; Zubkov, V. G.; Tyutyunnik, A. P.; Tarakina, N. V.; Surat, L. L.; Koryakova, O. V.; Vovkotrub, E. G. Upconversion luminescence in Er^{3+}/Yb^{3+} codoped $Y_2CaGe_4O_{12}$. *J. Alloys Compd.* **2011**, *509*, 1339−1346.

(20) Melkozerova, M. A.; Tarakina, N. V.; Maksimova, L. G.; Tyutyunnik, A. P.; Surat, L. L.; Leonidov, I. I.; Zubkov, V. G.; Zabolotskaya, E. V.; Samigullina, R. F. Application of a modified Pechini method for the synthesis of $Ln_2MGe_4O_{12}$ optical hosts. *J. Sol-Gel Sci. Technol.* **2011**, *59*, 338.

(21) Tarakina, N. V.; Zubkov, V. G.; Leonidov, I. I.; Tyutyunnik, A. P.; Surat, L. L.; Hadermann, J.; van Tendeloo, G. Crystal structure of the group of optical materials $Ln_2MeGe_4O_{12}$ (Me = Ca, Mn). *Zeitschrift für Kristallographie* **2009**, *2009*, 401−406.

(22) Zubkov, V. G.; Leonidov, I. I.; Tyutyunnik, A. P.; Tarakina, N. V.; Baklanova, I. V.; Perelyaeva, L. A.; Surat, L. L. Crystal structure and optical properties of germanates $Ln_2Ca(GeO_3)_4$ (Ln = Gd, Ho, Er, Yb, Y). *Phys. Solid State* **2008**, *50*, 1699−1706.

(23) Zubkov, V. G.; Tarakina, N. V.; Leonidov, I. I.; Tyutyunnik, A. P.; Surat, L. L.; Melkozerova, M. A.; Zabolotskaya, E. V.; Kellerman, D. G. Synthesis and crystal structure of $Ln_2M^{2+}Ge_4O_{12}$, Ln = rare-earth element or Y; M = Ca, Mn, Zn. *J. Solid State Chem.* **2010**, *183*, 1186−1193.

(24) Yamane, H.; Tanimura, R.; Yamada, T.; Takahashi, J.; Kajiwara, T.; Shimada, M. Synthesis and crystal structures of $CaY_2Ge_3O_{10}$ and $CaY_2Ge_4O_{12}$. *J. Solid State Chem.* **2006**, *179*, 289−295.

(25) Liu, X.-Q.; Battle, P. D.; Ridout, J.; Xu, D.; Ramos, S. Structural chemistry and magnetic properties of $Y_2CoGe_4O_{12}$. *J. Solid State Chem.* **2015**, *228*, 183−188.

(26) Rietveld, H. M. Profile refinement method for nuclear and magnetic structures. *J. Appl. Crystallogr.* **1969**, *2*, 65.

(27) Larson, A. C.; von-Dreele, R. B. *General Structure Analysis System (GSAS);* Technical Report LAUR 86−748; Los Alamos National Laboratories, 1994.

(28) van Laar, B.; Yelon, W. B. The Peak in Neutron Powder Diffraction. *J. Appl. Crystallogr.* **1984**, *17*, 47−54.

(29) Momma, K.; Izumi, F. VESTA: a three-dimensional visualization system for electronic and structural analysis. *J. Appl. Crystallogr.* **2008**, *41*, 653−658.

(30) Shannon, R. D. Revised effective ionic radii and systematic studies of interatomic distances in halides and chalcogenides. *Acta Crystallogr., Sect. A: Cryst. Phys., Diffr., Theor. Gen. Crystallogr.* **1976**, *A32*, 751.

(31) Sasaki, S.; Fujino, K.; Takeuchi, Y. X-ray determination of electron-density distributions in oxides, MgO, MnO, CoO, and NiO, and atomic scattering factors of their constituent atoms. *Proc. Jpn. Acad., Ser. B* **1979**, *55*, 43−48.

(32) Kummerle, E. A.; Heger, G. The structures of C-$Ce_2O_{3+\delta}$, Ce_7O_{12}, and $Ce_{11}O_{20}$. *J. Solid State Chem.* **1999**, *147*, 485−500.

(33) Hope, D. A. O.; Cheetham, A. K. A low-temperature powder neutron-diffraction study of the anti-ferromagnetic phase of $Mn_xCo_{1-x}O$. *J. Solid State Chem.* **1988**, *72*, 42−51.

DOI: 10.1021/acs.inorgchem.6b02905
Inorg. Chem. XXXX, XXX, XXX−XXX

(34) Dai, D.; Whangbo, M. H.; Koo, H. J.; Rocquefelte, X.; Jobic, S.; Villesuzanne, A. Analysis of the spin exchange interactions and the ordered magnetic structures of lithium transition metal phosphates $LiMPO_4$ (M = Mn, Fe, Co, Ni) with the olivine structure. *Inorg. Chem.* **2005**, *44*, 2407−2413.
(35) Whangbo, M. H.; Dai, D.; Koo, H. J. Spin dimer and classical spin analyses of the ordered magnetic structures of alkali iron pyrophosphates $NaFeP_2O_7$ and $LiFeP_2O_7$. *Dalton Trans.* **2004**, *2004*, 3019−3025.
(36) Ben Yahia, H.; Shikano, M.; Tabuchi, M.; Kobayashi, H.; Avdeev, M.; Tan, T. T.; Liu, S.; Ling, C. D. Synthesis and Characterization of the Crystal and Magnetic Structures and Properties of the Hydroxyfluorides Fe(OH)F and Co(OH)F. *Inorg. Chem.* **2014**, *53*, 365−374.
(37) Viola, M. C.; Martinez-Lope, M. J.; Alonso, J. A.; Martinez, J. L.; de Paoli, J. M.; Pagola, S.; Pedregosa, J. C.; Fernandez-Diaz, M. T.; Carbonio, R. E. Structure and magnetic properties of Sr_2CoWO_6: An ordered double perovskite containing Co^{2+}(HS) with unquenched orbital magnetic moment. *Chem. Mater.* **2003**, *15*, 1655−1663.
(38) Wallington, F.; Arevalo-Lopez, A. M.; Taylor, J. W.; Stewart, J. R.; Garcia-Sakai, V.; Attfield, J. P.; Stock, C. Spin-orbit transitions in alpha- and gamma-CoV_2O_6. *Phys. Rev. B: Condens. Matter Mater. Phys.* **2015**, *92*, 125116.
(39) David, R.; Kabbour, H.; Colis, S.; Mentre, O. Slow spin dynamics between ferromagnetic chains in a pure inorganic framework. *Inorg. Chem.* **2013**, *52*, 13742−13750.
(40) Wang, X. Y.; Wang, L.; Wang, Z. M.; Su, G.; Song, G. Coexistence of spin-canting, metamagnetism, and spin-flop in a (4,4) layered manganese azide polymer. *Chem. Mater.* **2005**, *17*, 6369−6380.

DOI: 10.1021/acs.inorgchem.6b02905
Inorg. Chem. XXXX, XXX, XXX−XXX